IDENTIFICATION OF HSV-1-INDUCED PLAQUE-LIKE FEATURE FORMATION ON A 3D NEURAL STEM CELL CULTURE MODEL OF ALZHEIMER'S DISEASE

Ian Lau

Department of Biomedical Engineering, Tufts University

Maria Savvidou, Ph. D.: Laidlaw Mentor

September 12, 2023

Abstract

Alzheimer's Disease (AD) is a neurodegenerative disorder that affects over 50 million individuals worldwide (Breijyeh & Karaman, 2020). While no known cures for AD currently exist, various medications and management strategies can reduce the severity of symptoms such as short-term memory loss and disorientation (Yiannopoulou & Papageorgiou, 2020). Pathological hallmarks of AD include the development of amyloid plaques and neurofibrillary tangles in the brain, contributing to the deleterious effects of AD (Serrano-Pozo et al., 2011). To better understand the metabolic dysfunction associated with AD development, two-photon excited fluorescence (TPEF) will be utilized in a novel 3D brain-like model of AD. Previous work conducted by the Georgakoudi group has demonstrated that the natural TPEF of two key coenzymes, NAD(P)H and FAD can be employed to perform metabolic assessments of cell activity through the redox ratio, mitochondrial clustering, and fluorescence lifetime (Liu et al., 2018) This study establishes an initial confocal image acquisition protocol by using 2D human induced neural stem cell (hiNSC) cultures for final application on a 3D brain-like model of AD. Optimizing this procedure will enable us to conduct future analysis with the 3D brain-like model of AD in a non-destructive and efficient manner, allowing us to better characterize the dynamic metabolic changes that occur throughout disease development.

Background

Alzheimer's Disease (AD) is a progressive, neurodegenerative disorder that is characterized by severe cognitive decline, short-term memory loss, and the inability to independently function in day-to-day activities (Breijyeh & Karaman, 2020). Currently over 50 million individuals are afflicted with AD worldwide, with sporadic or late-onset AD making up 95% of these patients (Cairns et al., 2020). Despite making great strides in dementia research, researchers have continued to grapple with its complex etiology. Consequently, no known cures for AD currently exist, although medication and management strategies can help alleviate symptoms associated with the disease (Yiannopoulou & Papageorgiou, 2020).

AD studies have previously identified the formation of neurofibrillary tangles (NFTs) and senile amyloid plaques as pathological hallmarks of the neurodegenerative disorder (Serrano-Pozo et al., 2011). Hyperphosphorylation of the microtubule-associated protein Tau results in the aggregation of NFTs in the brain. Senile amyloid plaques (Aß plaques) form through the clustering of ß-amyloid peptide, which is a cleavage product of the essential transmembrane protein amyloid precursor protein (APP) (Mattson, 2004). Functional APP has been implicated in neuron growth and synapse formation (Weyer et al., 2011). However, APP can also undergo sequential cleavage with ß and γ-secretase, where the formation of Aß41-42 peptide can occur. This fragmented Aß41-42 isoform has the potential to oligomerize into fibrils that ultimately contribute to the formation of neurotoxic and insoluble senile plaques that resist degradation (Butterfield & Halliwell, 2019). These Aß proteins are suggested to be causative agents of neuronal degeneration and neural network dysfunction, which finally result in familiar symptoms of AD such as memory decline and cognitive impairment (Chen et al., 2018) Thus, in vivo imaging of Aß plaque deposition in the brain is crucial for better understanding the pathology and development of AD.

Spatial imaging techniques such as PET and fMRI have been used as standard tools for assessing metabolic function in the human body (Sun et al., 2020; Zhu et al., 2015). However, inherent involvement of contrast agents and other labels limit the dynamic monitoring capabilities of these methods. Two-photon excited fluorescence (TPEF) has recently emerged as a label-free, high-resolution imaging acquisition method that has been utilized by various groups to analyze metabolic changes associated with AD development and plaque formation (Luo et al., 2022). Previous work conducted by the Georgakoudi group has demonstrated that the natural TPEF of two key coenzymes, NAD(P)H and FAD can be leveraged to perform optical assessment of metabolic activity through three key biomarkers: the redox ratio, fluorescence lifetime, and mitochondrial clustering (Liu et al., 2018). When utilized in tandem with one another, the aforementioned optical biomarkers serve as a crucial tool for extracting structural and functional insight related to the metabolic perturbation involved in disease development.

In order to elucidate the metabolic dysfunction resulting from Aß41-42-induced oxidative stress, non-destructive TPEF imaging of a novel, in-vitro engineered disease tissue model will be performed. This 3D brain-like model consists of a silk-collagen hybrid hydrogel embedded with human induced neural stem cells (hiNSCs). Recent experiments performed by the Kaplan Lab have demonstrated that tissue infection with low levels of herpes simplex virus type I (HSV-1) yields a brain-like model that exhibits the formation of Aß plaque-like formations (PLFs), neuronal loss, and other AD-like characteristics (Cairns et al., 2020). This preliminary study aims to establish an efficient image acquisition protocol with 2D hiNSC monolayer cultures before the 3D brain-like tissue model will be used. Optimizing this TPEF imaging acquisition method will ultimately enable us to better understand and characterize the dynamic metabolic changes that occur throughout AD development.

Methodology

Establishing a monolayer culture

Human foreskin fibroblasts were plated in a six-well plate before being cultured in fibroblast media [Dulbecco's modified Eagle's medium (DMEM), 10% fetal bovine serum, and 1% antibiotic-antimycotic]. Cells were infected at a MOI of 0.0001 before fibroblast media was exchanged to hiNSC media. On Day 4, cells were trypsinized to prepare them for plating on mouse embryonic fibroblast (MEF) feeder layers. hiNSC media was replaced every 1 to 3 days. Approximately 4 weeks later, colonies were selected to be replated onto new MEF feeder plates to generate a new hiNSC line. hiNSCs were passaged as colonies with trypsin-like enzyme, expanded, and frozen to produce stocks. All lines reported negative mycoplasma contamination.

3D brain-like tissue model of AD

A 3D brain-like tissue model of AD was established as previously described in *A 3D human brain-like tissue model of herpes-induced Alzheimer's disease* (Cairns et al., 2020). To produce scaffolds for the brain-like tissue model, silk sponges were generated using 6% (w/v) *Bombyx mori*-derived silk solution. Each sponge was biopsy-punched to form donut-shaped scaffolds (2-mm center hole). Scaffolds were autoclaved before being seeded with the dissociated hiNSCs and allowed to attach overnight. 3D brain-like tissue constructs were cultured in neurobasal media for 4 weeks to allow for maturation. Mature constructs were subsequently infected with HSV-1 with media being substituted every 3 days.

hiNSC Differentiation and Infection

hiNSC cultures were differentiated and infected as previously described (Cairns et al., 2020). Cell culture colonies were removed from the MEF feeder layers using trypsin-like enzyme and dissociated with manual pipetting. Subsequent cell suspensions were strained before the dissociated hiNSCs were cultured on ibidi 8-well gelatin-coated plates containing neurobasal media. HSV-1 was utilized to directly infect the hiNSCs at various MOIs (1×10^{-5} to 1) based on the starting virus concentration (2×10^{7} PFU/ml) and initial seeding density. Cell cultures were infected for the duration of the entire experiment to simulate low-level brain infection. For the mock infection control, an equal volume of control culture medium from uninfected cells was used. All virus experiments were approved by the Tufts Institutional Biosafety Committee.

Plaque-like formation (PLF) Staining

AlexaFluor647 (AF647) at Ex650/Em671 is a bright red, fluorescent dye with high photostability. hiNSC monocultures were stained with AF647 conjugated to Aß peptides to label low abundance plaque-like formations.

PLF Identification with live AF647 staining:

Images were acquired using a Leica TCS SP8 confocal microscope. ROIs were first identified by performing a preliminary scan of each specimen using the 10x air objective. The microscope was adjusted to locate the best imaging depth for locating plaque-like formations (PLFs). After identifying the PLF, further adjustments were made to center the ROI in the field of view. The X, Y, and Z positions were recorded before the microscope was switched to a 20x air objective. Under 20x magnification, the prerecorded coordinates were used to locate the same ROI before new coordinates were registered. Finally, the microscope was switched to a 40x water-immersion objective.

Results

Initially, hiNSCs cells were grown on monolayer cultures followed by HSV-1 infection for seven days. Aß plaques were stained with AF-647 conjugated antibody and confocal images were acquired at 10x, 20x and 40x magnification. This established protocol was subsequently applied to the identification of Aß PLFs in the 3D brain-like tissue model. Silk used for the development of the 3D cultures was verified using DAPI stain and subsequently identified using the Leica TCS SP8 confocal microscope. Figure 1 exhibits the presence and growth of plaque-like-features in areas around the cells.

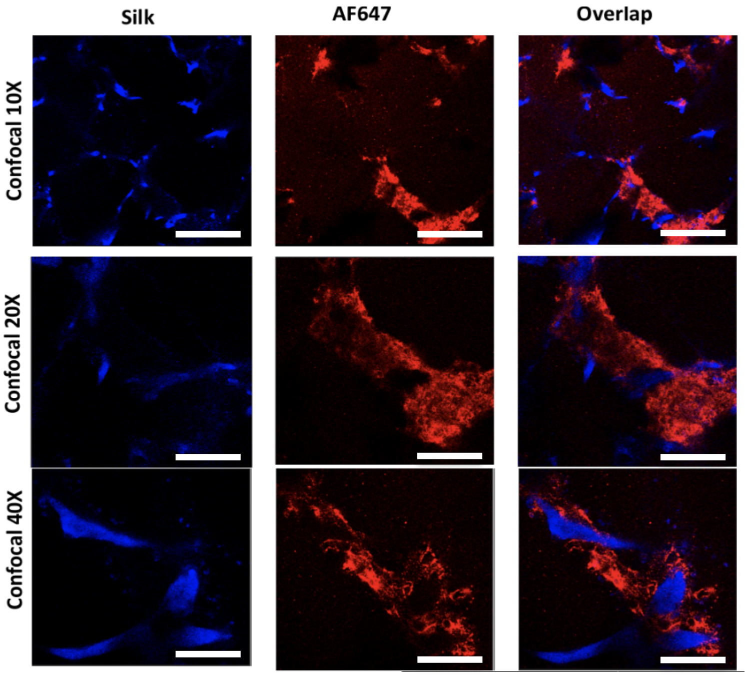

Figure 1. Images were acquired of the hiNSC 3D cultures stained with AF647 antibodies conjugated to the Aβ^+ PLFs (red color). Silk was identified on the DAPI channel (blue color). Magnification was gradually increased to 40x to locate PLF formation in the silk. (*SB = 50 μm*).

Discussion

hiNSC cultures infected with HSV-1 demonstrated gradual development of plaque-like formations (PLFs) after incubation (Figure 1). To pinpoint the exact location and development of the PLFs, a region of interest (ROI) was selected through a preliminary scan of the scaffold at 10x objective magnification. The microscope was adjusted to establish the best imaging depth before the X, Y, and Z coordinates were recorded. This procedure was repeated at 20x air and 40x water objective magnification to localize the PLF at the center of the ROI (Figure 1, red fluorescence).

By establishing a PLF-identification protocol for 2D hiNSC cultures and verifying the ability of this protocol to identify PLFs within a 3D culture, future work will enable us to authenticate TPEF as a reliable and efficient imaging acquisition method that can correspondingly be utilized to analyze the 3D brain-like tissue model of AD. Ultimately, optimizing this protocol serves as a novel method of identifying PLF development in a more robust model of the neurodegenerative disease, allowing us to further understand its metabolic development and pathophysiology.

References

Breijyeh, Z., & Karaman, R. (2020). Comprehensive Review on Alzheimer's Disease: Causes and Treatment. *Molecules (Basel, Switzerland)*, *25*(24), 5789. https://doi.org/10.3390/molecules25245789

Butterfield, D. A., & Halliwell, B. (2019). Oxidative stress, dysfunctional glucose metabolism and Alzheimer disease. *Nature reviews. Neuroscience*, *20*(3), 148–160. https://doi.org/10.1038/s41583-019-0132-6

Cairns, D. M., Rouleau, N., Parker, R. N., Walsh, K. G., Gehrke, L., & Kaplan, D. L. (2020). A 3D human brain-like tissue model of herpes-induced Alzheimer's disease. *Science advances*, *6*(19), eaay8828. https://doi.org/10.1126/sciadv.aay8828

Chen, C., Liang, Z., Zhou, B., Li, X., Lui, C., Ip, N. Y., & Qu, J. Y. (2018). In Vivo Near-Infrared Two-Photon Imaging of Amyloid Plaques in Deep Brain of Alzheimer's Disease Mouse Model. *ACS chemical neuroscience*, *9*(12), 3128–3136. https://doi.org/10.1021/acschemneuro.8b00306

Liu, Z., Pouli, D., Alonzo, C. A., Varone, A., Karaliota, S., Quinn, K. P., Münger, K., Karalis, K. P., & Georgakoudi, I. (2018). Mapping metabolic changes by noninvasive, multiparametric, high-resolution imaging using endogenous contrast. *Science advances*, *4*(3), eaap9302. https://doi.org/10.1126/sciadv.aap9302

Luo, Z., Xu, H., Samanta, S., Zhang, R., Luo, G., Wang, Y., Liu, L., Weng, X., He, J., Liao, C., Wang, Y., Guo, B., & Qu, J. (2022). Long-Term Repeatable In Vivo Monitoring of Amyloid-β Plaques and Vessels in Alzheimer's Disease Mouse

Model with Combined TPEF/CARS Microscopy. *Biomedicines*, *10*(11), 2949. https://doi.org/10.3390/biomedicines10112949

Mattson M. P. (2004). Pathways towards and away from Alzheimer's disease. *Nature*, *430*(7000), 631–639. https://doi.org/10.1038/nature02621

Serrano-Pozo, A., Frosch, M. P., Masliah, E., & Hyman, B. T. (2011). Neuropathological alterations in Alzheimer disease. *Cold Spring Harbor perspectives in medicine*, *1*(1), a006189. https://doi.org/10.1101/cshperspect.a006189

Sun, X., Nie, B., Zhao, S., Ai, L., Chen, Q., Zhang, T., Pan, T., Wang, L., Yin, X., Zhang, W., Shan, B., Liu, H., Liang, S., & Wang, G. (2020). Distinct relationships of amyloid-beta and tau deposition to cerebral glucose metabolic networks in Alzheimer's disease. *Neuroscience letters*, *717*, 134699. https://doi.org/10.1016/j.neulet.2019.134699

S. W. Weyer, M. Klevanski, A. Delekate, V. Voikar, D. Aydin, M. Hick, M. Filippov, N. Drost, K. L. Schaller, M. Saar, M. A. Vogt, P. Gass, A. Samanta, A. Jäschke, M. Korte, D. P. Wolfer, J. H. Caldwell, U. C. Müller, APP and APLP2 are essential at PNS and CNS synapses for transmission, spatial learning and LTP. EMBO J. 30, 2266–2280 (2011).

Yiannopoulou K.G., Papageorgiou S.G. Current and future treatments in alzheimer disease: An update. *J. Cent. Nerv. Syst. Dis.* 2020:12. doi: 10.1177/1179573520907397.

Zhu, X. H., Lu, M., Lee, B. Y., Ugurbil, K., & Chen, W. (2015). In vivo NAD assay reveals the intracellular NAD contents and redox state in healthy human brain and their age dependences. *Proceedings of the National Academy of Sciences of* *the United States of America*, *112*(9), 2876–2881.

https://doi.org/10.1073/pnas.1417921112